

On a spatial-Temporal Decomposition of Optical Flow

Aniello Raffaele Patrone Otmar Scherzer

May 16, 2022

ANIELLO RAFFAELE PATRONE

Computational Science Center
University of Vienna
Oskar-Morgenstern Platz 1, 1090 Vienna, Austria

OTMAR SCHERZER

Computational Science Center
University of Vienna
Oskar-Morgenstern Platz 1, 1090 Vienna, Austria
and
Johann Radon Institute for Computational and Applied Mathematics
(RICAM)
Altenbergerstraße 69, 4040 Linz, Austria

Abstract

In this paper we present a spatial-temporal variational decomposition algorithm for computation of the optical flow of a dynamic image sequence. We consider several applications, such as the extraction of temporal motion patterns of different scales and motion detection in dynamic sequences under varying illumination conditions, such as they appear for instance in psychological flickering experiments. For the numerical implementation we are solving an *integro-differential* equation by a fixed point iteration. For comparison purposes we use the standard time dependent optical flow algorithm, which in contrast to our method, constitutes in solving a spatial-temporal *differential* equation.

1 Introduction

Analyzing the motion in a dynamic sequence is of interest in many fields of applications, like human computer interaction, medical imaging, psychology, to mention but a few. In this paper we study the extraction of motion in dynamic sequences by means of the optical flow, which is the apparent motion of objects, surfaces, and edges in a dynamic visual scene caused by the relative motion between an observer and the scene. There have been proposed several computational approaches for optical flow computations in the literature. In this paper we emphasize on variational methods. In this research area the first method is due to Horn & Schunck [15]. Like many alternatives and generalizations, this

methods calculates the flow from two consecutive frames. Here, we are calculating the optical flow from all frames simultaneously. Spatial-temporal optical flow methods were previously studied by Weickert & Schnörr [28, 29], [11], [26] and [2], to name but a few. However, in contrast to these paper we emphasize on the *decomposition* of the optical flow into appropriate components.

Variational modeling of patterns in *stationary* images has been initialized with the seminal book of Y. Meyer [20]. In the context of total variation regularization, reconstructions of patterns was studied first in [24]. Here, we are implementing similar ideas as have been used before for variational image denoising [3, 4, 5, 6, 7, 13, 25] and optical flow decomposition [1, 18, 30, 31, 32]. However, a conceptual difference is that we aim for extracting *temporal* patterns, and in all the mentioned papers the decomposition was with respect to the space component. We emphasize that the proposed method is one of very few variational optical flow algorithms in a space-time regime. Within this class, this algorithm is the only spatial-temporal *decomposition* algorithm.

The outline of this paper is as follows: In Section 2 we review the optical flow equation. In Section 3 we present analytical examples of the optical flow equation in case of illumination disturbances. In Section 4 we introduce the new model for spatial-temporal optical flow decomposition. We formulate it as a minimization problem and derive the optimality conditions for a minimizer. In Section 5 we make calculations, which help to understand the decomposition algorithm from an analytical point of view. In Section 6 we derive a fixed point algorithm for numerical minimization of the energy functional. Finally in Section 7 and Section 8 we present experiments, results and a discussion of them.

2 Registration and optical flow

The problem of aligning dynamic sequences $f(\cdot, t)$ can be formulated as the operator equation, of finding a flow Ψ of diffeomorphisms,

$$\Psi(\cdot, t) : \Omega \rightarrow \Omega, \quad \forall t \in [0, T],$$

such that

$$f(\Psi(\vec{x}, t), t) = f(\vec{x}, 0), \quad \forall \vec{x} \in \Omega \text{ and } t \in [0, T]. \quad (1)$$

For natural images, in general, it is not possible to solve equation (1) subject to the constraint that Ψ is a diffeomorphism for every t , because of occlusions, illumination changes, noise, and information gain/loss in the movie over time. Thus the optical flow and image registration community typically do not consider this constraint, in contrast to the shape registration community (see for instance [9, 16]).

Differentiation of (1) with respect to t for a fixed \vec{x} gives

$$\nabla f(\Psi(\vec{x}, t), t) \cdot \partial_t \Psi(\vec{x}, t) + \partial_t f(\Psi(\vec{x}, t), t) = 0, \quad \forall \vec{x} \in \Omega \text{ and } t \in [0, T]. \quad (2)$$

Switching from a Lagrangian to an Eulerian description allows to define the *optical flow equation (OFE)* on Ω :

$$\nabla f(\vec{x}, t) \cdot \vec{u}(\vec{x}, t) + \partial_t f(\vec{x}, t) = 0, \quad \forall \vec{x} \in \Omega \text{ and } t \in [0, T]. \quad (3)$$

In particular this means that (3) is not well-motivated on subsets of Ω which are not met by a characteristic curve in space and time starting from $t = 0$. This problem is less relevant if the optical flow equation is considered for just two consecutive frames, which is the standard optical flow approach in the literature. In this case, a characteristic originates always at some point Ω through the re-initialization at each pair of frames. Instead of solving (3) usually the relaxed problem is considered, which consists in minimizing the functional

$$S(\vec{u}) := \int_{\Omega} (\nabla f(\vec{x}, t) \cdot \vec{u}(\vec{x}, t) + \partial_t f(\vec{x}, t))^2 d\vec{x} \rightarrow \min, , \quad \forall t \in [0, T] \quad (4)$$

subject to appropriate constraints.

3 The optical flow equation in case of illumination disturbances

In this section we are showing simple motivating examples explaining properties of the solution of the optical flow equation (3) under changing illumination conditions.

Example 1 *We consider the 1D optical flow equation, to solve for u in*

$$\partial_x f(x, t)u(x, t) + \partial_t f(x, t) = 0 \text{ in } (0, 1) \times (0, 1) \quad (5)$$

for the specific data

$$f(x, t) = \tilde{f}(x)g(t) \text{ for } (x, t) \in (0, 1) \times (0, 1). \quad (6)$$

f represents a dynamic sequence with brightness variation, g over time. We are more specific and take:

$$\tilde{f}(x) = x(1 - x) \text{ and } g(t) = 1 - t. \quad (7)$$

The function f and the level lines are plotted in Figure 1 and the optical flow can be explicitly calculated:

$$u(x, t) = \frac{x(1 - x)}{1 - 2x} \frac{1}{1 - t}$$

indicates a transport of intensities from outside to the center $1/2$. We observe that $u(1/2, t)$ and $u(x, 1)$ are singularities of the optical flow. From the definition of u it follows that

$$\hat{u}(x, t) := \int_0^t u(x, \tau) d\tau = -\frac{x(1 - x)}{1 - 2x} \log(1 - t),$$

and thus

$$\begin{aligned} \|\hat{u}\|_{L^2((0,1)^2)}^2 &= \int_0^1 \frac{x^2(1 - x)^2}{(1 - 2x)^2} dx \int_0^1 \log^2(1 - t) dt \\ &= 2 \int_0^1 \frac{x^2(1 - x)^2}{(1 - 2x)^2} dx = \infty, \end{aligned}$$

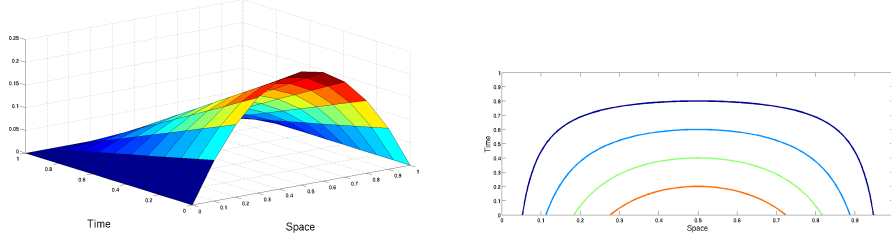


Figure 1: $f(x, t) = x(1 - x)(1 - t)$ from (7). Level lines of f are parametrized by $(\Psi(x, t), t)$.

or in other words $u \notin L^2((0, 1)^2)$. In contrast, constraining the equation to a compact domain C of $(0, 1/2)$ in space $u \in L^2(C \times (0, 1))$.

The deformation Ψ of the non-linear optical flow equation is given by

$$\Psi(x, t) = \frac{1}{2} \pm \sqrt{\frac{1}{4} - \frac{x(1-x)}{1-t}} \text{ for } t \leq 4 \left(x - \frac{1}{2}\right)^2,$$

where the branch of Ψ with $+$ is active if $x > 1/2$ and the other branch holds for $x < 1/2$. Moreover, we have

$$\partial_t \Psi(x, t) = \mp \frac{x(1-x)}{\sqrt{1-t-4x(1-x)}} \frac{1}{(1-t)^{3/2}}.$$

This shows that the flow has a singularity (endpoint) at $t = 1 - 4x(1-x)$.

In Figure 2 there are shown u and $\partial_t \Psi$. Along characteristics (initiated at $t = 0$) the optical flow equation produces the same results as the registration equation. However, note that $\Psi(x, t)$ satisfies the equation

$$\partial_x f(\Psi(x, t), t) \partial_t \Psi(x, t) + \partial_t f(\Psi(x, t), t) = 0,$$

which in comparison to (3) evaluates f at space locations $\Psi(x, t)$ instead of x and $\partial_t \Psi$ and u have to be compared at different space positions in the domain, which are covered by characteristics.

We expect that a collapse of characteristics manifest itself in less smoothness of the optical flow. In fact such situations appear in practical situations when occlusions are recorded.

Example 2 We consider input data f of the form (6) with

$$\tilde{f}(x) = x(1-x) \text{ and } g(t) = \exp \left\{ -\frac{1}{\beta}(1-t)^\beta \right\} \text{ with some } 0 < \beta < 1 \quad (8)$$

for $(x, t) \in \hat{\Omega} := (0, 1/4) \times (0, 1)$. The optical flow is given by

$$u(x, t) = -\frac{x(1-x)}{1-2x} (1-t)^{\beta-1}.$$

Integrating this function over time gives

$$\hat{u}(x, t) := \int_0^t u(x, \tau) d\tau = \frac{x(1-x)}{1-2x} \frac{1}{\beta} ((1-t)^\beta - 1),$$

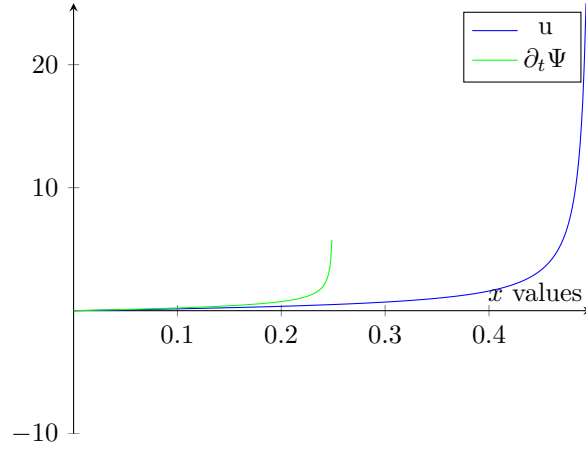


Figure 2: Linear versus non-linear optical flow: u and $\partial_t \Psi$ at $t = 1/4$. Note that $\partial_t \Psi$ is only defined in the interval $[0, 1/4]$, which is plotted, while u is defined for $[0, 1/2)$.

and consequently with

$$C := \frac{1}{\beta^2} \int_0^{1/4} \frac{x^2(1-x)^2}{(1-2x)^2} dx < \infty,$$

we get

$$\begin{aligned} \|u\|_{L^2(\hat{\Omega})}^2 &= C \int_0^1 t^{2\beta-2} dt = \begin{cases} C \frac{1}{2\beta-1} & \text{if } \beta > \frac{1}{2}, \\ \infty & \text{else.} \end{cases} \\ \|\hat{u}\|_{L^2(\hat{\Omega})}^2 &= C \int_0^1 t^{2\beta} - 2t^\beta + 1 dt = \begin{cases} C \left(\frac{1}{2\beta+1} - \frac{2}{\beta+1} + 1 \right) & \text{if } \beta > -\frac{1}{2}, \\ \infty & \text{else.} \end{cases} \end{aligned}$$

This shows that for $0 < \beta < 1/2$ $u \notin L^2(\hat{\Omega})$ but $\hat{u} \in L^2(\hat{\Omega})$.

The bottom line of these examples is that illumination changes, such as flickering, may result in singularities of the optical flow and a violation of standard smoothness assumptions of the optical flow field. The potential appearance of the singularities motivates us to consider regularization terms for optical flow computations, which allow for singularities over time, such as negative Sobolev norms or G -norms.

4 Optical flow decomposition: basic setup and formalism

In this paper we derive an optical flow model for decomposing the flow field into spatial and temporal components. We consider the frames defined on a two-dimensional domain and in order to minimize the number of constants we

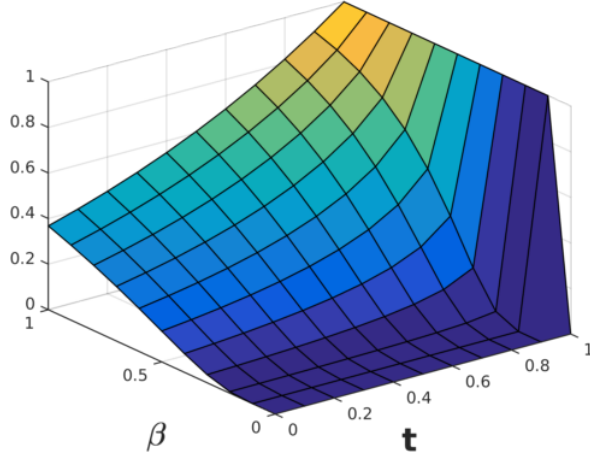


Figure 3: $g(t) = \exp \left\{ -\frac{1}{\beta}(1-t)^\beta \right\}$

take in (3) the time-interval $(0, 1)$ and $\Omega = (0, 1)^2$. We assume that the optical flow field to be a compound of two flow field components

$$\vec{u}(\vec{x}, t) = \vec{u}^{(1)}(\vec{x}, t) + \vec{u}^{(2)}(\vec{x}, t) = \begin{pmatrix} u_1^{(1)}(\vec{x}, t) \\ u_2^{(1)}(\vec{x}, t) \end{pmatrix} + \begin{pmatrix} u_1^{(2)}(\vec{x}, t) \\ u_2^{(2)}(\vec{x}, t) \end{pmatrix}.$$

Because there appears a series of indices and variables it is convenient to specify the notation first:

$\vec{x} = (x_1, x_2)$	Euclidean space
$\partial_k = \frac{\partial}{\partial x_k}$	Differentiation with respect to spatial variable x_k
$\partial_t = \frac{\partial}{\partial t}$	Differentiation with respect to time
$\nabla = (\partial_1, \partial_2)^T$	Gradient in space
$\nabla_3 = (\partial_1, \partial_2, \partial_t)^T$	Gradient in space and time
$\nabla \cdot = \partial_1 + \partial_2$	Divergence in space
$\nabla_3 \cdot = \partial_1 + \partial_2 + \partial_t$	Divergence in space and time
\vec{n}	normal vector to Ω
f	input sequence
$f(\cdot, t)$	movie frame
$\vec{u}^{(i)}$	optical flow module, $i = 1, 2$
$\vec{u} = \vec{u}^{(1)} + \vec{u}^{(2)}$	optical flow
$u_j^{(i)}$	j -th optical flow component of the i -th module
$\Psi^{(i)}$	components of deformation,
$\Psi = \Psi^{(1)} + \Psi^{(2)}$	total deformation
$\hat{u}(\cdot, t) = \int_0^t u(\cdot, \tau) d\tau$	Primitive of u
$\hat{\hat{u}}(\cdot, t) = - \int_t^1 \hat{u}(\cdot, \tau) d\tau$	2nd Primitive of u - note $\partial_t \hat{\hat{u}}(\cdot, t) = \hat{u}(\cdot, t)$

The OFE-equation (3) contains four unknown (real valued) functions $u_j^{(i)}$, $i, j = 1, 2$, and thus is highly under-determined. To overcome the lack of equations, the problem is formulated as a constrained optimization problem, to de-

termine, for some fixed $\alpha > 0$,

$$\operatorname{argmin} \left(\mathcal{R}^{(1)}(\vec{u}^{(1)}) + \alpha \mathcal{R}^{(2)}(\vec{u}^{(2)}) \right) \quad (9)$$

subject to (3). Here $\mathcal{R}^{(i)}$, $i = 1, 2$ are convex, non-negative functionals, such that $\mathcal{R}^{(1)} + \alpha \mathcal{R}^{(2)}$ is strictly convex. Instead of solving the constrained optimization problem, we use a soft variant and minimize the unconstrained regularization functional:

$$\begin{aligned} \mathcal{F}(\vec{u}^{(1)}, \vec{u}^{(2)}) &:= \mathcal{E}(\vec{u}^{(1)}, \vec{u}^{(2)}) + \sum_{i=1}^2 \alpha^{(i)} \mathcal{R}^{(i)}(\vec{u}^{(i)}), \\ \mathcal{E}(\vec{u}^{(1)}, \vec{u}^{(2)}) &:= \int_{\Omega \times (0,1)} (\nabla f \cdot (\vec{u}^{(1)} + \vec{u}^{(2)}) + \partial_t f)^2 d\vec{x} dt \text{ with } \alpha = \frac{\alpha^{(2)}}{\alpha^{(1)}}. \end{aligned} \quad (10)$$

In the following we design the regularizers $\mathcal{R}^{(i)}$. Moreover, for the sake of simplicity of presentation, we omit the space and time arguments of the functions $u_j^{(i)}$ and f , whenever it simplifies the formulas without possible misinterpretations.

- For $\mathcal{R}^{(1)}$ we use a common spatial-temporal regularization functional for optical flow regularization (see for instance [29]):

$$\mathcal{R}^{(1)}(\vec{u}^{(1)}) := \int_{\Omega \times (0,1)} \nu \left(\left| \nabla_3 u_1^{(1)} \right|^2 + \left| \nabla_3 u_2^{(1)} \right|^2 \right) d\vec{x} d\tau, \quad (11)$$

where $\nu : [0, \infty) \rightarrow [0, \infty)$ is a monotonically increasing, differentiable function. For the choice of ν we follow [29] and take

$$\nu(r) = \epsilon r + (1 - \epsilon) \lambda^2 \sqrt{1 + \frac{r}{\lambda^2}}, \forall r \in [0, \infty), \quad (12)$$

with $0 < \epsilon \ll 1$ and $\lambda > 0$. The function $r \rightarrow \nu \circ (r \rightarrow r^2)$ is convex in r and there exist constants $c_1, c_2 > 0$ with $c_1 r^2 \leq \nu(r) \leq c_2 r^2$ for all $r \in \mathbb{R}$. Moreover, we denote by ν' the derivative of ν .

- $\mathcal{R}^{(2)}$ is designed to penalize for variations of the second component in time. Motivated by Y. Meyer's book [20], we introduce a regularization term, which is non-local in *time*. We have seen in Example 1 that u may violate L^2 -smoothness in case of changing illumination conditions. Variations of Meyer's G -norm were used in energy functionals for calculating *spatial* decompositions of the optical flow [1, 17]. It is a challenge to compute the G -norm efficiently, and therefore workarounds have been proposed. For instance [24] proposed as an alternative at the G -norm the following realization for the H^{-1} norm: For a generalized function $u : (0, 1) \rightarrow \mathbb{R}$, they defined

$$\|u\|_{H^{-1}}^2 = - \int_0^1 u(t) \partial_{tt}^{-1} u(t) dt.$$

Here, we use this workaround for a realization for the *temporal* H^{-1} -norm, which we use as a regularization functional:

$$\mathcal{R}^{(2)}(\vec{u}^{(2)}) := \int_{\Omega \times (0,1)} \left| \int_0^t \vec{u}^{(2)}(\vec{x}, \tau) d\tau \right|^2 d\vec{x} dt = \sum_{j=1}^2 \int_{\Omega \times (0,1)} \left(\widehat{u}_j^{(2)}(\vec{x}, t) \right)^2 d\vec{x} dt. \quad (13)$$

To see the analogy with the $\|\cdot\|_{H^{-1}}$ -norm from [24] we note that the second primitive of the optical flow component $\vec{u}^{(2)}$, satisfies for $j = 1, 2$ and $\vec{x} \in \Omega$

$$\widehat{u}_j^{(2)}(\vec{x}, 1) = 0, \quad \partial_t \widehat{u}_j^{(2)}(\vec{x}, 0) = \widehat{u}_j^{(2)}(\vec{x}, 0) = 0. \quad (14)$$

Then, by integration by parts it follows that

$$- \int_0^1 \underbrace{\widehat{u}_j^{(2)}(t)}_{=\partial_{tt}^{-1} u_j^{(2)}} u_j^{(2)}(t) dt = \int_0^1 \left(\widehat{u}_j^{(2)}(t) \right)^2 dt$$

and therefore

$$\mathcal{R}^{(2)}(\vec{u}^{(2)}) = \sum_{j=1}^2 \int_{\Omega} \left\| u_j^{(2)}(\vec{x}, \cdot) \right\|_{H^{-1}}^2 d\vec{x}. \quad (15)$$

4.1 Energy functional and minimization

We are determining the optimality conditions for minimizers of \mathcal{F} introduced in (10). Necessary conditions for a minimizer are that the directional derivatives vanish for all 2-dimensional vector valued functions $\vec{h}^{(j)} : \Omega \times (0, 1) \rightarrow \mathbb{R}^2$, $j = 1, 2$. To formulate these conditions we use the simplifying notation:

$$(\mathcal{E}, \mathcal{F}) := (\mathcal{E}, \mathcal{F})(\vec{u}^{(1)}, \vec{u}^{(2)}), \mathcal{R}^{(i)} := \mathcal{R}^{(i)}(\vec{u}^{(i)}) \text{ and } \text{res} = \nabla f \cdot (\vec{u}^{(1)} + \vec{u}^{(2)}) + \partial_t f.$$

Therefore the directional derivative of \mathcal{F} in direction $\vec{u}^{(j)}$ is given by:

$$(\partial_{\vec{u}^{(j)}} \mathcal{F}) \vec{h}^{(j)} = \lim_{s \rightarrow 0} \frac{\mathcal{F}(\vec{u}^{(1)} + s\delta_{1j}\vec{h}^{(1)}, \vec{u}^{(2)} + s\delta_{2j}\vec{h}^{(2)}) - \mathcal{F}}{s} = 0$$

where $\delta_{ij} = 1$ for $i = j$ and zero else is the Kronecker symbol. The gradient of the functional \mathcal{F} from (10) can be determined by calculating the directional derivatives of \mathcal{E} and $\mathcal{R}^{(i)}$, separately.

- The directional derivative of \mathcal{E} in direction $\vec{h}^{(j)}$ is given by

$$(\partial_{\vec{u}^{(j)}} \mathcal{E}) \vec{h}^{(j)} = 2 \int_{\Omega \times (0,1)} \text{res} \nabla f \cdot \vec{h}^{(j)} d\vec{x} dt. \quad (16)$$

- The directional derivative of $\mathcal{R}^{(1)}$ at $\vec{u}^{(1)}$ in direction $\vec{h}^{(1)}$ is determined as follows: Let us abbreviate for simplicity of presentation

$$\nu := \nu \left(\left| \nabla_3 u_1^{(1)} \right|^2 + \left| \nabla_3 u_2^{(1)} \right|^2 \right), \quad \nu' := \nu' \left(\left| \nabla_3 u_1^{(1)} \right|^2 + \left| \nabla_3 u_2^{(1)} \right|^2 \right),$$

then the directional derivative of $\mathcal{R}^{(1)}$ in direction $\vec{h}^{(1)}$ at $\vec{u}^{(1)}$ is given by

$$\begin{aligned}
(\partial_{\vec{u}^{(1)}} \mathcal{R}^{(1)}) \vec{h}^{(1)} &= \lim_{s \rightarrow 0} \frac{\mathcal{R}^{(1)}(\vec{u}^{(1)} + s \vec{h}^{(1)}) - \mathcal{R}^{(1)}}{s} \\
&= \lim_{s \rightarrow 0} \frac{1}{s} \int_{\Omega \times (0,1)} \nu \left(\left| \nabla_3(u_1^{(1)} + s h_1^{(1)}) \right|^2 + \left| \nabla_3(u_2^{(1)} + s h_2^{(1)}) \right|^2 \right) - \nu \, d\vec{x} dt \\
&= -2 \int_{\Omega \times (0,1)} \nabla_3 \cdot \left(\nu' \nabla_3 u_1^{(1)} \right) h_1^{(1)} + \nabla_3 \cdot \left(\nu' \nabla_3 u_2^{(1)} \right) h_2^{(1)} d\vec{x} dt,
\end{aligned} \tag{17}$$

where integration by parts is used to prove the final identity.

- The directional derivative of $\mathcal{R}^{(2)}$ is derived as follows:

$$\begin{aligned}
(\partial_{\vec{u}^{(2)}} \mathcal{R}^{(2)}) \vec{h}^{(2)} &= \lim_{s \rightarrow 0} \frac{\mathcal{R}^{(2)}(\vec{u}^{(2)} + s \vec{h}^{(2)}) - \mathcal{R}^{(2)}}{s} \\
&= \lim_{s \rightarrow 0} \frac{1}{s} \int_{\Omega \times (0,1)} \left(\left| \int_0^t \vec{u}^{(2)} + s \vec{h}^{(2)} d\tau \right|^2 - \left| \int_0^t \vec{u}^{(2)} d\tau \right|^2 \right) d\vec{x} dt \\
&= 2 \sum_{j=1}^2 \int_{\Omega \times (0,1)} \widehat{u}_j^{(2)} \widehat{h}_j^{(2)} d\vec{x} dt.
\end{aligned} \tag{18}$$

Moreover, it follows by integration by parts of the last line of (18) with respect to t that

$$(\partial_{\vec{u}^{(2)}} \mathcal{R}^{(2)}) \vec{h}^{(2)} = -2 \sum_{j=1}^2 \int_{\Omega \times (0,1)} \widehat{u}_j^{(2)}(\vec{x}, t) h_j^{(2)}(\vec{x}, t) d\vec{x} dt. \tag{19}$$

Now, because of (17) and (16) it follows that the minimizer $\vec{u}^{(i)}$, $i = 1, 2$ has to satisfy for every $j = 1, 2$,

$$\begin{aligned}
\partial_j f(\nabla f \cdot (\vec{u}^{(1)} + \vec{u}^{(2)}) + \partial_t f) - \alpha^{(1)} \nabla_3 \cdot \left(\nu' \nabla_3 u_j^{(1)} \right) &= 0 \text{ in } \Omega \times (0, 1), \\
\partial_{\vec{n}} u_j^{(1)} &= 0 \text{ in } \partial\Omega \times (0, 1), \\
\partial_t u_j^{(1)} &= 0 \text{ in } \Omega \times \{0, 1\}.
\end{aligned} \tag{20}$$

Because of (16) and (19) hold for all $\vec{h}_j^{(2)}$, it follows that for every $j = 1, 2$,

$$\partial_j f(\nabla f \cdot (\vec{u}^{(1)} + \vec{u}^{(2)}) + \partial_t f) - \alpha^{(2)} \widehat{u}_j^{(2)} = 0 \text{ in } \Omega \times (0, 1). \tag{21}$$

Thus the optimality conditions for a minimizer are (20) and (21).

5 Optical flow decomposition in 1D

In order to make transparent the features of our decomposition we study exemplarily the 1D case again. From regularization theory (see e.g. [23]) we know that the minimizers $(u_{\vec{\alpha}}^{(1)}, u_{\vec{\alpha}}^{(2)})$, for $\vec{\alpha} = (\alpha^{(1)}, \alpha^{(2)}) \rightarrow 0$, are converging to a solution of the optical flow equation which minimizes

$$\mathcal{R} = \mathcal{R}^{(1)} + \alpha \mathcal{R}^{(2)} \text{ for } \alpha = \lim_{\vec{\alpha} \rightarrow 0} \frac{\alpha^{(2)}}{\alpha^{(1)}} > 0.$$

Such a solution is called \mathcal{R} minimizing solution. Note that by the 1D simplification the modules $u^{(i)}$, $i = 1, 2$ are single valued functions.

We calculate the decomposition for the optical flow equation (5), for the specific test data (6). The regularized solutions approximate the \mathcal{R} minimizing solution, and thus these calculations can be viewed representative for the properties of the minimizer of the regularization method. For these particular kind of data the solution of the optical flow equation is given by :

$$u(x, t) = -\frac{\tilde{f}(x)}{\partial_x \tilde{f}(x)} \frac{\partial_t g(t)}{g(t)} = -\frac{\partial_t (\log g)(t)}{\partial_x (\log \tilde{f})(x)}. \quad (22)$$

Let us assume that $(\log g)(t) - (\log g)(0)$ can be expanded into a Fourier sin-series:

$$(\log g)(t) - (\log g)(0) = \int_0^t \partial_t (\log g)(\tau) d\tau = \sum_{n=1}^{\infty} \hat{g}_n \sin(n\pi t). \quad (23)$$

Moreover, we assume that $1/\partial_x (\log \tilde{f})(x)$ can be expanded in a cos-series:

$$\frac{1}{\partial_x (\log \tilde{f})(x)} = \sum_{m=0}^{\infty} f_m \cos(m\pi x). \quad (24)$$

Then

$$-\frac{(\log g)(t) - (\log g)(0)}{\partial_x (\log \tilde{f})(x)} = \hat{u}(x, t) = \hat{u}_1(x, t) + \hat{u}_2(x, t). \quad (25)$$

Inserting this identity in the regularization functional

$$\mathcal{R}(u^{(1)}, u^{(2)}) = \int_{(0,1) \times (0,1)} (\partial_x u^{(1)})^2 + (\partial_t u^{(1)})^2 + \alpha \left(\hat{u}^{(2)} \right)^2 dx dt,$$

we remove the $u^{(2)}$ dependence, and we get

$$\mathcal{R}(\hat{u}^{(1)}) := \int_{(0,1) \times (0,1)} (\partial_{xt} \hat{u}^{(1)})^2 + (\partial_{tt} \hat{u}^{(1)})^2 + \alpha \left(\frac{(\log g)(t) - (\log g)(0)}{\partial_x (\log \tilde{f})(x)} + \hat{u}^{(1)} \right)^2 dx dt,$$

where we enforce the following boundary conditions on $\hat{u}^{(1)}$: From the definition of $\hat{u}^{(1)}$ it follows that $\hat{u}^{(1)}(x, 0) = 0$. Secondly, we enforce $\hat{u}^{(1)}(x, 1) = 0$. In fact, the assumption is reasonable because of the choice of \hat{g} , when the series $\sum_{n=0}^{\infty} \hat{g}_n$ is absolutely convergent, $\hat{g}(1) = 0$, which implies that $\hat{u}^{(1)}(x, 1) + \hat{u}^{(2)}(x, 1) = 0$, which is guaranteed in particular by $\hat{u}^{(1)}(x, 1) = \hat{u}^{(2)}(x, 1) = 0$.

By substituting the relation between $\hat{u}^{(2)}$ and $\hat{u}^{(1)}$ we reduce the constraint optimization problem to an unconstrained optimization problem for $\hat{u}^{(1)}$, and the minimizer solves the partial differential equation

$$\partial_{ttxx} \hat{u}^{(1)} + \partial_{tttt} \hat{u}^{(1)} + \alpha \left(\frac{(\log g)(t) - (\log g)(0)}{\partial_x (\log \tilde{f})(x)} + \hat{u}^{(1)} \right) = 0 \text{ in } (0, 1) \times (0, 1),$$

together with the boundary conditions:

$$\begin{aligned} \partial_{tt} \hat{u}^{(1)} &= \hat{u}^{(1)} = 0 \text{ on } (0, 1) \times \{0, 1\}, \\ \partial_x \partial_{tt} \hat{u}^{(1)} &= 0 \text{ on } \{0, 1\} \times (0, 1). \end{aligned} \quad (26)$$

Now, we substitute $\hat{w} := \partial_{tt}\hat{u}^{(1)}$, and we get the following system of equations

$$\begin{aligned}\partial_{xx}\hat{w} + \partial_{tt}\hat{w} &= -\alpha \left(\frac{(\log g)(t) - (\log g)(0)}{\partial_x(\log \hat{f})(x)} + \hat{u}^{(1)} \right) \text{ in } (0, 1) \times (0, 1), \\ \hat{w} &= 0 \text{ on } (0, 1) \times \{0, 1\}, \\ \partial_x\hat{w} &= 0 \text{ on } \{0, 1\} \times (0, 1).\end{aligned}\tag{27}$$

and

$$\hat{u}^{(1)}(x, t) = \int_0^t \int_0^\tau \hat{w}(x, \hat{\tau}) d\hat{\tau} d\tau - t \int_0^1 \int_0^\tau \hat{w}(x, \hat{\tau}) d\hat{\tau} d\tau.$$

\hat{w} can be expanded as follows:

$$\hat{w}(x, t) = \sum_{m, n=0}^{\infty} \hat{w}_{mn} \cos(m\pi x) \sin(n\pi t),$$

and we expand $\hat{u}^{(1)}$ in an analogous manner:

$$\hat{u}^{(1)}(x, t) = \sum_{m, n=0}^{\infty} \hat{u}_{mn}^{(1)} \cos(m\pi x) \sin(n\pi t),$$

such that

$$\hat{w}_{mn} = -n^2 \pi^2 \hat{u}_{mn}^{(1)}, \quad \forall m, n \in \mathbb{N}_0.\tag{28}$$

Thus it follows from (27) that

$$\hat{w}_{mn}(m^2 + n^2)\pi^2 = \alpha \left(\hat{u}_{mn}^{(1)} + f_m \hat{g}_n \right), \quad \forall m, n \in \mathbb{N}_0.\tag{29}$$

(28) and (29) imply that

$$\hat{u}_{mn}^{(1)} = -\frac{\alpha}{\alpha + \pi^4(m^2 + n^2)n^2} f_m \hat{g}_n, \quad \forall m, n \in \mathbb{N}_0.\tag{30}$$

Now, consider a specific test example $g(t) = \exp \left\{ \frac{\sin(n_0 \pi t)}{n_0 \pi} \right\}$ for some $n_0 \in \mathbb{N}$. Then, from (22) it follows that $u(x, t) = -\frac{\cos(n_0 \pi t)}{\partial_x(\log \hat{f})(x)}$, and correspondingly we have

$$(\log g)(t) - (\log g)(0) = \frac{\sin(n_0 \pi t)}{n_0 \pi} = \sum_{n=1}^{\infty} \frac{\delta_{nn_0}}{n_0 \pi} \sin(n\pi t).$$

In this case it follows from (30) that

$$\hat{u}_{mn}^{(1)} = -\frac{\alpha}{\alpha + \pi^4(m^2 + n_0^2)n_0^2} \frac{\delta_{nn_0}}{n_0 \pi} f_m.$$

For flickering $u^{(2)}$ is pronounced (if n_0 is large $\hat{u}_{mn}^{(1)} \approx 0$) while in the quasi-static case $u^{(1)}$ is dominant. Moreover, we also see that spatial components belonging to Fourier-cos coefficients with large m are more pronounced in the $u^{(2)}$ component, and the spatial and temporal coefficients are mixed.

$f = f(r, s, t) \in \mathbb{R}^{M \times N \times T}$	Input sequence
$\vec{u}^{(i)} = \vec{u}^{(i)}(r, s, t; k) \in \mathbb{R}^{M \times N \times T \times K \times 2}$	artificial optical flow module
$\vec{u}^{(i)} = \vec{u}^{(i)}(r, s, t) = \vec{u}^{(i)}(r, s, t; K)$ $\in \mathbb{R}^{M \times N \times T \times 2}$	formal relation between artificial and optical flow module
$u_j^{(i)} = u_j^{(i)}(r, s, t; k) \in \mathbb{R}^{M \times N \times T \times K}$	component of artificial optical flow module
$u_j^{(i)} = u_j^{(i)}(r, s, t) = u_j^{(i)}(r, s, t; K)$ $\in \mathbb{R}^{M \times N \times T}$	formal relation between components of artificial and optical flow module
∂_k^h	Finite difference approximation in direction x_k
∂_t^h	Finite difference approximation in direction t

Table 1: Discrete Notation

6 Numerics

In this section we discuss the numerical minimization of the energy functional \mathcal{F} defined in (10). Our approach is based on solving the optimality conditions for the minimizer $u_j^{(i)}$, $i, j = 1, 2$ from (20), (21) with a fixed point iteration. We call the iterates of the fixed point iteration $u_j^{(i)}(\vec{x}, t; k)$, for $k = 1, 2, \dots, K$, where K denotes the maximal number of iterations. We summarize all the iterates of the components of flow functions $u_j^{(i)}$ in a tensor of size $M \times N \times T \times K$. In this section we use the notation as reported in table 1. For every tensor $H = (H(r, s, t)) \in \mathbb{R}^{M \times N \times T}$ (representing a complete movie) we define the discrete gradient

$$\nabla_3^h H(r, s, t) = (\partial_1^h H(r, s, t), \partial_2^h H(r, s, t), \partial_t^h H(r, s, t))^T \text{ for } (r, s, t) \in \mathbb{R}^{M \times N \times T},$$

where

$$\begin{aligned} \partial_1^h H(r, s, t) &= \frac{H(r+1, s, t) - H(r-1, s, t)}{2\Delta_x} & \text{if } 1 < r < M \\ \partial_2^h H(r, s, t) &= \frac{H(r, s+1, t) - H(r, s-1, t)}{2\Delta_y} & \text{if } 1 < s < N \\ \partial_t^h H(r, s, t) &= \frac{H(r, s, t+1) - H(r, s, t-1)}{2\Delta_t} & \text{if } 1 < t < T \end{aligned} \quad (31)$$

and $\Delta_x = \frac{1}{M-1}$, $\Delta_y = \frac{1}{N-1}$ and $\Delta_t = \frac{1}{T-1}$. Again, whenever possible, we leave out the indices. Moreover, we define the discrete divergence, which is the adjoint of the discrete gradient: Let $(H_1, H_2, H_3)^T(r, s, t)$, then

$$\nabla_3^h \cdot (H_1, H_2, H_3)^T = \partial_1^h H_1 + \partial_2^h H_2 + \partial_t^h H_3. \quad (32)$$

The realization of the fixed point iteration for solving the discretized equations (20) and (21) reads as follows:

- $k = 0$: we initialize two flow components $\vec{u}^{(1)}(\cdot; 0), \vec{u}^{(2)}(\cdot; 0) \in \mathbb{R}^{M \times N \times K \times 2}$.
- $k \rightarrow k + 1$: let $\nu^{(k)} := \nu'(|\nabla_3^h u_1^{(1)}(\cdot; k)|^2 + |\nabla_3^h u_1^{(2)}(\cdot; k)|^2)$, then

$$\begin{aligned} \frac{u_1^{(1)}(\cdot; k+1) - u_1^{(1)}(\cdot; k)}{\Delta_\tau} &= \nabla_3^h \cdot \left(\nu^{(k)} \nabla_3^h u_1^{(1)}(\cdot; k) \right) \\ &\quad - \frac{\partial_1^h f}{\alpha^{(1)}} \left[\partial_1^h f \left(u_1^{(1)}(\cdot; k+1) + u_1^{(2)}(\cdot; k) \right) \right. \\ &\quad \left. + \partial_2^h f \left(u_2^{(1)}(\cdot; k) + u_2^{(2)}(\cdot; k) \right) + \partial_t^h f \right], \end{aligned} \quad (33)$$

$$\begin{aligned} \frac{u_2^{(1)}(\cdot; k+1) - u_2^{(1)}(\cdot; k)}{\Delta_\tau} &= \nabla_3^h \cdot \left(\nu^{(k)} \nabla_3^h u_2^{(1)}(\cdot; k) \right) \\ &\quad - \frac{\partial_2^h f}{\alpha^{(1)}} \left[\partial_1^h f \left(u_1^{(1)}(\cdot; k+1) + u_1^{(2)}(\cdot; k) \right) \right. \\ &\quad \left. + \partial_2^h f \left(u_2^{(1)}(\cdot; k+1) + u_2^{(2)}(\cdot; k) \right) + \partial_t^h f \right], \end{aligned} \quad (34)$$

$$\begin{aligned} \frac{u_1^{(2)}(\cdot; k+1) - u_1^{(2)}(\cdot; k)}{\Delta_\tau} &= \widehat{u}_1^{(2)}(\cdot; k) \\ &\quad - \frac{\partial_1^h f}{\alpha^{(2)}} \left[\partial_1^h f \left(u_1^{(1)}(\cdot; k+1) + u_1^{(2)}(\cdot; k+1) \right) \right. \\ &\quad \left. + \partial_2^h f \left(u_2^{(1)}(\cdot; k+1) + u_2^{(2)}(\cdot; k) \right) + \partial_t^h f \right], \end{aligned} \quad (35)$$

and

$$\begin{aligned} \frac{u_2^{(2)}(\cdot; k+1) - u_2^{(2)}(\cdot; k)}{\Delta_\tau} &= \widehat{u}_2^{(2)}(\cdot; k) \\ &\quad - \frac{\partial_2^h f}{\alpha^{(2)}} \left[\partial_1^h f \left(u_1^{(1)}(\cdot; k+1) + u_1^{(2)}(\cdot; k+1) \right) \right. \\ &\quad \left. + \partial_2^h f \left(u_2^{(1)}(\cdot; k+1) + u_2^{(2)}(\cdot; k+1) \right) + \partial_t^h f \right], \end{aligned} \quad (36)$$

where

$$\widehat{u}_j^{(2)}(r, s, t; k) = - \sum_{\tau=t}^1 \sum_{\tilde{\tau}=0}^{\tau} u_j^{(2)}(r, s, \tilde{\tau}; k), \quad j = 1, 2.$$

and Δ_τ is the step size parameter, which has been set to 10^{-4} .

The system (33),(34),(35),(36) can be solved efficiently using the special structure of the matrix equation similarly to [28, 29].

The iterations are stopped when the Euclidean norm of the relative error

$$\frac{|u_j^{(i)}(\cdot, k) - u_j^{(i)}(\cdot, k+1)|}{|u_j^{(i)}(\cdot, k)|}, \quad j = 1, 2$$

drops below the precision tolerance value $tol = 0.05$ for at least one of the component of $\vec{u}^{(1)}$ and one of $\vec{u}^{(2)}$. The typical number of iterations is much below 100.

7 Experiments

In this section we present numerical experiments to demonstrate the potential of the proposed optical flow decomposition model. In the first two experiments we use for visualization of the computed flow fields the standard flow color coding [8]. The flow vectors are represented in color space via the color wheel illustrated in Figure 4. For the third and fourth experiment we use a black and white visualization technique. There black is assigned to pixels where no flow is present and a gray-shade elsewhere, which is proportional to the flow magnitude. In order to compare frequencies of the sequences used for testing

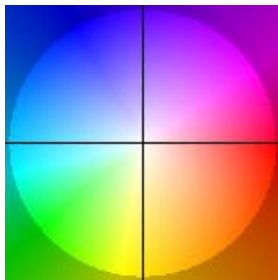


Figure 4: Color Wheel.

all the intensity values of f are scaled in the range $(0, 1)$. The used parameters are reported for each experiment except for $\Delta_x, \Delta_y, \Delta_t$ defined as in Section 6. In this work we consider the following four dynamic image sequences:

- The first experiment is performed with the video sequence from [19] (available at <http://of-eval.sourceforge.net/>) which consists of forty-six frames showing a rotating sphere with some overlaid patterns. The analytical results from Section 5 in 1D show that the intensity of the $\vec{u}^{(2)}$ component increases monotonically with increasing frequency over time. We verify this hypothesis numerically in higher dimensions. We simulate in particular two, four and eight times the original motion frequency. In order to do so, we duplicate the sequence periodically, however consider it to be in the same time interval $(0, 1)$. The flow visualized in Figure 5 is the one between the 16th and the 17th frame of every sequence. We study the behavior of the sphere at different motion frequencies with the same parameter setting $\alpha^{(1)} = 1$, $\alpha^{(2)} = \frac{1}{4}$. The numerical results confirm the 1D observation that for high frequency movement $\vec{u}^{(2)}$ is dominant (cf. Figures 5) and $\vec{u}^{(1)}$ is always 20% of $\vec{u}^{(2)}$.
- The second experiment concerns the decomposition of the motion in a dynamic image sequence showing a projection of a cube moving over an oscillating background. The movie consists of sixty frames and can be viewed on the web-page <http://www.csc.univie.ac.at/index.php?page=visualattention>. The background is oscillating in diagonal direction, from the bottom left to the top right, with a periodicity of four frames. In each frame the oscillation has a rate of 5% of the frame size. The flow visualized in Figure 6 is the one between the 20th and the 21st frame of the sequence. Applying

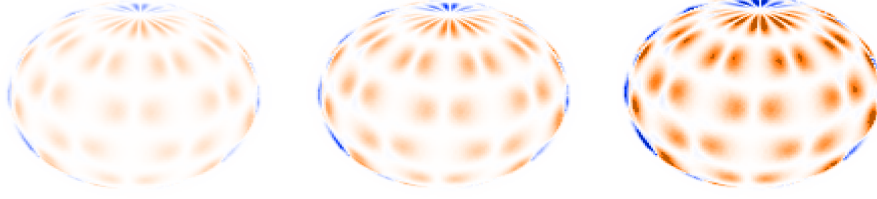


Figure 5: $\vec{u}^{(2)}$ at different frequencies of rotations: 2, 4 and $8\times$ faster than the original motion frequency. $\alpha^{(1)} = 1$, $\alpha^{(2)} = \frac{1}{4}$. The intensity of $\vec{u}^{(2)}$ increases when the frequency of rotation is increased.

the proposed method with a parameter setting $\alpha^{(1)} = 10^3$, $\alpha^{(2)} = 10^3$, $\Delta_\tau = 10^{-5}$, and precision tolerance $tol = 0.001$, we notice that the background movement appears almost solely in $\vec{u}^{(2)}$ and the global movement of the cube appears in $\vec{u}^{(1)}$. In Figure 6 we represent only flow vectors with magnitude larger than 0.05 and omit in $\vec{u}^{(2)}$ the part in common with $\vec{u}^{(1)}$ for better visibility.

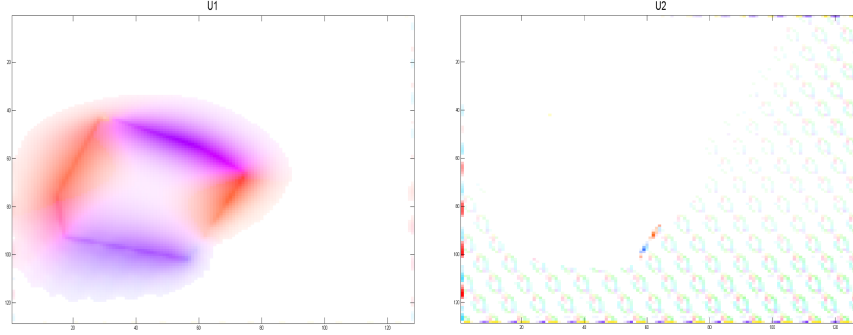


Figure 6: The dynamic sequence consists of the smooth (translation like) motion of a cube and an oscillating background. The oscillation has a periodicity of four frames and takes place along the diagonal direction from the bottom left to the top right, moving at a rate of 5% of the frame size in each frame. The proposed model decomposes the motion, obtaining the global movement of the cube in $\vec{u}^{(1)}$ (left) and the background movement solely in $\vec{u}^{(2)}$ (right).

- In the third experiment the original movie consists of thirty-two frames and can be viewed together with the decomposition result on the web-page <http://www.csc.univie.ac.at/index.php?page=visualattention>. The flow is decomposed into two components. The first part shows the movement of a Ferris wheel and people walking. The second part shows blinking lights and the reflection of the wheel. The flow visualized in Figure 7 is the one between the 4th and the 5th frame of the sequence with a parameter setting $\alpha^{(1)} = 1$, $\alpha^{(2)} = \frac{1}{4}$. In order to improve the visibility we represent only flow vectors with magnitude larger than 0.18 and we omit in $\vec{u}^{(2)}$ the part in common with $\vec{u}^{(1)}$.



Figure 7: $\vec{u}^{(1)}$: Movement of a Ferris wheel and people walking in the foreground (top left). $\vec{u}^{(2)}$ consists of blinking lights and the reflections of the wheel (top right). The third image (bottom) is a reference frame.

- The fourth example is flickering. In a standard flickering experiment, the difference in human attention is investigated by inclusion of blank images in a repetitive image sequence. Although, in general, these blank images are not deliberately recognized, they change the awareness of the test persons. J. K. O'Regan [22] states that “*Change blindness is a phenomenon in which a very large change in a picture will not be seen by a viewer, if the change is accompanied by a visual disturbance that prevents attention from going to the change location*”. They provided test data <http://nivea.psych.univ-paris5.fr>, which we used for our simulations. The proposed optical flow decomposition is able to detect regions, which also humans can recognize, but standard optical flow algorithms fail to: To show this the input sequence is composed by four frames consisting of Frame 1, a blank image, Frame 2 and again an identical blank image (see Figure 9 (top)). This sequence is then aligned periodically to a movie. We interpret the movie as a linear interpolation between the frames.

We test and compare Horn-Schunck, Weickert-Schnörr and the proposed algorithm. We set the smoothness parameter $\alpha^{(1)}$ to a value of one for all the methods. Moreover, for our approach we set $\alpha^{(2)} = 1$. For Horn-Schunck we visualize the flow field in Figure 8. This flow is the one between the blank frame and the slightly changed frame, which exceeds a threshold of 3.9. The results obtained by applying Weickert-Schnörr and the $\vec{u}^{(1)}$ field of our approach, respectively, are small in magnitude. Therefore, we do not visualize them. This behavior is coherent with the motivation of the Weickert-Schnörr method to produce an optical flow that is less sensitive to variations over space and time. Finally, we visualize in Figure 9 (down right) the $\vec{u}^{(2)}$ flow field for the proposed approach. For the visualization we omit all vectors with magnitude lower than 0.18. In

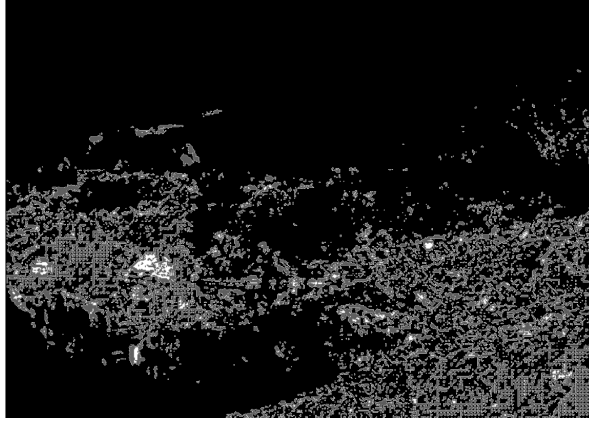


Figure 8: Result with Horn-Schunck

order to make transparent the result, we show in Figure 9 (down left) the difference between the two frames of the sequence containing information (see Figure 9 (top)). In this experiment, we notice that the $\vec{u}^{(1)}$ component is negligible, instead $\vec{u}^{(2)}$ detects the areas affected by change of intensities (see Figure 9 (down right)).

7.1 Additional Information

In the following, we show the capacity of our model to extract more and different information compared to standard optical flow algorithms. The current literature focuses on average angular and endpoint error [8] in order to compare optical flow algorithms. Our model extracts information, that is neglected by standard algorithms. Such difference can be shown through a quantitative comparison of models. For this purpose, we use well-known test sequences from the Middlebury database <http://vision.middlebury.edu/flow/>, and evaluate the residual of the *optical flow constraint*. We compare the residual of our method with the one of the Horn-Schunck method [15]. However, the Horn-Schunck method does not take into account time information, and therefore we calculate for every pair of successive frames and stack the series of flow images into a movie. For calculating the flow for one pair we use the regularization parameter $\alpha = 400$ and 50 iterations for every pair of frames. For the proposed method $\alpha^{(1)} = 400$, $\alpha^{(2)} = 10$ and tolerance value $tol = 0.03$. In this case the whole image sequence is used at once.

The parameters $\alpha^{(1)}, \alpha^{(2)}$ are chosen larger than 1 in order to avoid overfitting. For every pair of successive images f_1 and f_2 we visualize the squared residual

$$\int_{\Omega} \left(\nabla f_1 \cdot \vec{u} + \frac{f_2 - f_1}{\Delta_t} \right)^2 d\vec{x},$$

both for Horn-Schunck and the proposed method. Note that for the comparison we omit space dependency of the movie. We notice from Figure 10 that the squared residual is larger in every frame for Horn-Schunck than for our decomposition model, meaning that the proposed method is capable to extract more flow information.

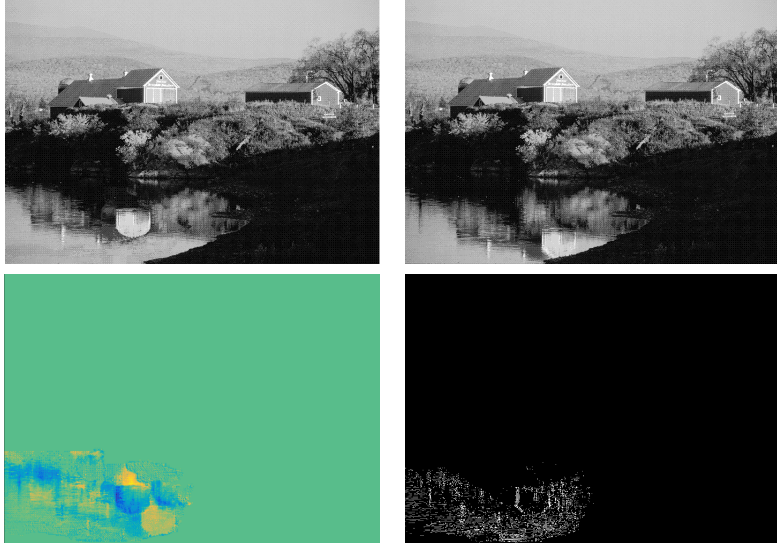


Figure 9: The two frames of the flickering sequence containing information (top), the difference between these two frames (down left), and the $\vec{u}^{(2)}$ flow field resulting from the proposed approach (down right). As predicted in sections 3 and 5 the $\vec{u}^{(1)}$ component is negligible, instead $\vec{u}^{(2)}$ detects the change of intensity across the blank sheet.

	Weickert-Schnörr	Proposed model
Hamburg Taxi	1374.9	1021
RubberWhale	4459.7	3046.8
Hydrangea	8533.3	7647.2
DogDance	9995.4	8217.6
Walking	8077.5	5944.3

Table 2: Comparison of squared residuals over space and time \mathcal{E} between Weickert-Schnörr and the proposed method.

In order to understand how much information our method is capable to extract from an entire dynamic sequence, we also calculate the residual squared over space and time: $\mathcal{E}(\vec{u}^{(1)}, \vec{u}^{(2)})$ as in (10) and compare it with the squared residual over space and time of the Weickert-Schnörr method [28, 29]. We use the parameter settings $\alpha^{(1)} = 100$ ($\alpha = \alpha^{(1)}$ in Weickert-Schnörr) and $\alpha^{(2)} = \frac{1}{4}$, tolerance $tol = 0.01$, in order to have a good comparison of the two methods. Again the residual is smaller for the proposed method as shown in table 2.

8 Conclusion

We present a new optical flow model for decomposing the flow in spatial and temporal components of different scales. A main ingredient of our work is a new variational formulation of the optical flow equation. Finally, many applications

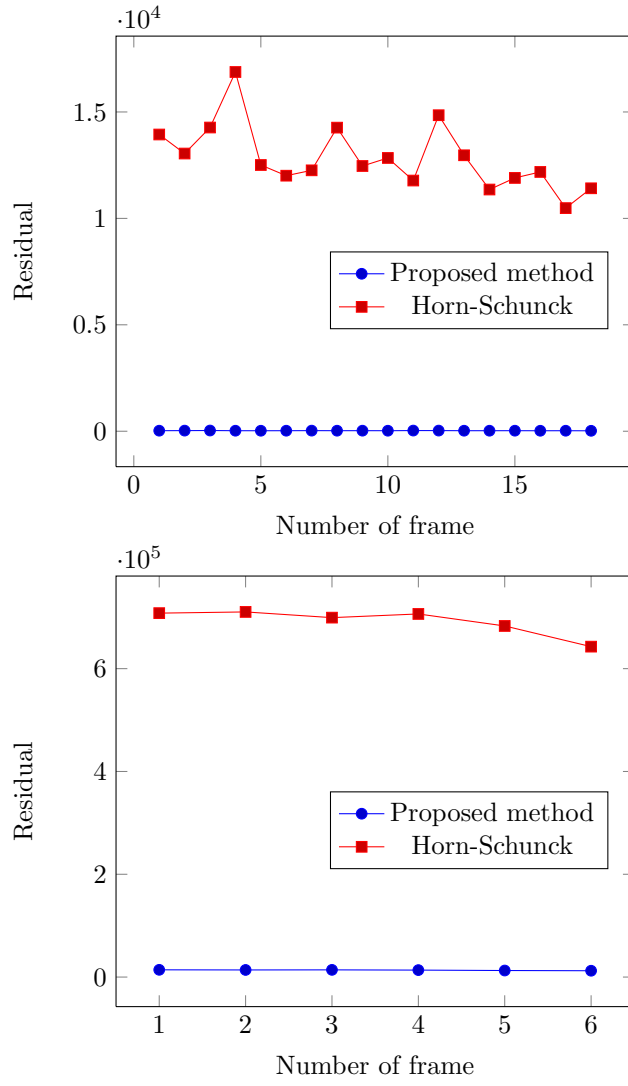


Figure 10: Residuals for Hamburg taxi (up) and Minicooper sequence (down) from Middlebury database. Residuals for Horn-Schunck are plotted in red, the proposed method is plotted in blue.

are considered both analytically and computationally in case of illumination disturbances.

Acknowledgment

This work is carried out within the project *Modeling Visual Attention as a Key Factor in Visual Recognition and Quality of Experience* funded by the Wiener Wissenschafts und Technologie Fonds - WWTF. OS is also supported by the Austrian Science Fund - FWF, Project S11704 with the national research network, NFN, Geometry and Simulation. The authors would like to thank U. Ansorge, C. Valuch, S. Buchinger, C. Kirisits, P. Elbau, L. Lang, G. Dong, T. Widlak for interesting discussions on the optical flow and José A. Iglesias for discussions and the creation of the cube sequence.

References

- [1] Abhau J, Belhachmi Z, Scherzer O On a decomposition model for optical flow. In: Energy Minimization Methods in Computer Vision and Pattern Recognition, Lecture Notes in Computer Science, vol 5681, Springer-Verlag, Berlin, Heidelberg, 2009, pp 126–139, DOI 10.1007/978-3-642-03641-5_10, URL http://dx.doi.org/10.1007/978-3-642-03641-5_10
- [2] Andreev R, Scherzer O and Zulehner W Simultaneous optical flow and source estimation: space-time discretization and preconditioning. RICAM-Report No. 2014-23, 2015 URL <https://www.ricam.oeaw.ac.at/publications/reports/14/rep14-23.pdf>
- [3] Aubert G, Aujol JF Modeling very oscillating signals. Application to image processing. Appl Math Optim 51(2), 2005, 163–182
- [4] Aujol JF, Chambolle A Dual norms and image decomposition models. Int J Comput Vision 63(1), 2005, 85–104
- [5] Aujol JF, Kang S Color image decomposition and restoration. J Vis Commun Image Represent 17(4), 2006, 916–928 DOI 10.1016/j.jvcir.2005.02.001, URL <http://www.sciencedirect.com/science/article/B6WMK-4FTWJGT-1/2/ffd97bf7a31e0b9cfdc8af0895369e84>
- [6] Aujol JF, Aubert G, Blanc-Féraud L, Chambolle A Image decomposition into a bounded variation component and an oscillating component. J Math Imaging Vision 22(1), 2005, 71–88
- [7] Aujol JF, Gilboa G, Chan T, Osher S Structure-texture image decomposition—modeling, algorithms, and parameter selection. Int J Comput Vision 67(1), 2006, 111–136
- [8] Baker S, Scharstein D, Lewis JP, Roth S, Black MJ, Szeliski R A database and evaluation methodology for optical flow. Int J Comput Vision 92(1), 2011, 1–31, DOI 10.1007/s11263-010-0390-2, URL <http://www.springerlink.com/index/10.1007/s11263-010-0390-2>

- [9] Bauer M, Bruveris M, Michor W.P. Overview of the geometries of shape spaces and diffeomorphism groups. *J Math Imaging Vision* 50(1-2), 2014, 60–97, DOI 10.1007/s10851-013-0490-z, URL <http://dx.doi.org/10.1007/s10851-013-0490-z>
- [10] Berkels B, Effland A and Rumpf M Time discrete geodesic paths in the space of images. *ArXiv* 2015 URL <http://arxiv.org/abs/1503.02001>
- [11] Borzi A, Ito K, and Kunisch K Optimal control formulation for determining optical flow. *SIAM J Sci Comput* 24(3), 2002, 818–847
- [12] Bruhn A Variational optic flow computation: Accurate modeling and efficient numerics. PhD thesis 2006, Saarland University, Germany
- [13] Duval V, Aujol JF, Vese L Mathematical modeling of textures: Application to color image decomposition with a projected gradient algorithm. *J Math Imaging Vision* 37, 2010, 232–248
- [14] Hanke M, Scherzer O Inverse problems light: numerical differentiation. *Amer. Math. Monthly* 108(6), 2001, 512–521 DOI 10.2307/2695705, URL <http://dx.doi.org/10.2307/2695705>
- [15] Horn BKP, Schunck BG Determining optical flow. *Artificial Intelligence* 17, 1981, 185–203
- [16] Jain A, Younes L A kernel class allowing for fast computations in shape spaces induced by diffeomorphisms. *J Comput and Applied Math* 245, 2013, 162–181 DOI 10.1016/j.cam.2012.10.019, URL <http://dx.doi.org/10.1016/j.cam.2012.10.019>
- [17] Kirisits C, Lukas L, Scherzer O Decomposition of optical flow on the sphere. *GEM-Int J on Geomathematics* 5(1), 2014, 117–141, DOI 10.1007/s13137-013-0055-8, URL <http://dx.doi.org/10.1007/s13137-013-0055-8>
- [18] Kohlberger T, Memin E, Schnörr C Variational dense motion estimation using the helmholtz decomposition. In: Griffin LD, Lillholm M (eds) *Scale Space Methods in Computer Vision, Lecture Notes in Computer Science*, vol 2695, Springer, Berlin, 2003, 432–448, DOI 10.1007/3-540-44935-3_30, URL http://dx.doi.org/10.1007/3-540-44935-3_30
- [19] McCane B, Novins K, Crannitch D, Galvin B On benchmarking optical flow. *Comput Vision Image Understanding* 84, 2001, 126–143
- [20] Meyer Y Oscillating patterns in image processing and nonlinear evolution equations, *University Lecture Series*, vol 22, 2001. American Mathematical Society, Providence, RI, the fifteenth Dean Jacqueline B. Lewis memorial lectures
- [21] Miller M I, Younes L Group actions, homeomorphisms, and matching: A general framework *Int J Comput Vision* 41(1/2), 2001, 61–84,
- [22] O'Regan JK Change blindness. *E Cognitive science*, 2007

- [23] Scherzer O, Grasmair M, Grossauer H, Haltmeier M, Lenzen F Variational methods in imaging, Applied Mathematical Sciences, vol 167, 2009. Springer, New York, DOI 10.1007/978-0-387-69277-7, URL <http://dx.doi.org/10.1007/978-0-387-69277-7>
- [24] Vese L, Osher S Modeling textures with total variation minimization and oscillating patterns in image processing. J Sci Comput 19(1–3), 2003, 553–572, special issue in honor of the sixtieth birthday of Stanley Osher
- [25] Vese L, Osher S Image denoising and decomposition with total variation minimization and oscillatory functions. J Math Imaging Vision 20, 2004, 7–18
- [26] Wang CM, Fan KC, Wang CT Estimating Optical Flow by Integrating Multi-Frame Information. Journal of Information Science and Engineering 24, 2008, 1719–1731
- [27] Weickert J, Bruhn A, Brox T, Papenberg N A Survey on Variational Optic Flow Methods for Small Displacements. Mathematical Models for Registration and Applications to Medical Imaging, Springer Berlin Heidelberg 10, 2006, 103–136 URL http://dx.doi.org/10.1007/978-3-540-34767-5_5
- [28] Weickert J, Schnörr C A theoretical framework for convex regularizers in PDE-based computation of image motion. Int J Comput Vision 45(3), 2001a, 245–264
- [29] Weickert J, Schnörr C Variational optic flow computation with a spatio-temporal smoothness constraint. J Math Imaging Vision 14, 2001b, 245–255
- [30] Yuan J, Schörr C, Steidl G Simultaneous higher-order optical flow estimation and decomposition. SIAM J Sci and Stat Comput 29(6), 2007, 2283–2304 (electronic), DOI 10.1137/060660709, URL <http://dx.doi.org/10.1137/060660709>
- [31] Yuan J, Steidl G, Schnörr C Convex Hodge decomposition of image flows. In: Pattern recognition, Lecture Notes in Comput. Sci., vol 5096, Springer, Berlin, 2008, 416–425, DOI 10.1007/978-3-540-69321-5_42, URL http://dx.doi.org/10.1007/978-3-540-69321-5_42
- [32] Yuan J, Schnörr C, Steidl G Convex Hodge decomposition and regularization of image flows. J Math Imaging Vision 33(2), 2009, 169–177, DOI 10.1007/s10851-008-0122-1, URL <http://dx.doi.org/10.1007/s10851-008-0122-1>